PCCP

PAPER

View Article Online
View Journal | View Issue

Published on 09 June 2016. Downloaded by University of Rochester on 07/07/2016 20:32:32.

Cite this: *Phys. Chem. Chem. Phys.*, 2016, **18**, 18227

Theoretical analysis of hot electron injection from metallic nanotubes into a semiconductor interface

Chathurangi S. Kumarasinghe,*[a] Malin Premaratne,*[a] Sarath D. Gunapala[b] and Govind P. Agrawal[c]

Received 6th May 2016,
Accepted 8th June 2016

DOI: 10.1039/c6cp03043b

www.rsc.org/pccp

Metallic nanostructures under optical illumination can generate a non-equilibrium high-energy electron gas (also known as hot electrons) capable of being injected into neighbouring media over a potential barrier at particle boundaries. The nature of this process is highly nanoparticle shape and size dependent. Here, we have derived an analytical expression for the frequency dependent rate of injection of these energetic electrons from a metallic nanotube into a semiconductor layer in contact with its inner boundary. In our derivation, we have considered the quantum mechanical motion of the electron gas confined by the particle boundaries in determining the electron energy spectrum and wave functions. We present a comprehensive theoretical analysis of how different geometric parameters such as the outer to inner radius ratio, length and thickness of a nanotube and illumination frequency affect the hot electron injection and internal quantum efficiency of the nanotube. We reveal that longer nanotubes with thin shells and high inner to outer radius ratios show better performance at visible and infrared frequencies. Our derivations and results provide the much needed theoretical insight for optimization of thin nanotubes for different hot electron based applications.

1 Introduction

When illuminated with light, electrons inside nanoparticles absorb photons and move to high-energy non-equilibrium states.[1,2] These high-energy electrons are referred to as hot electrons and a fraction of them often have sufficient momentum to cross the potential barrier at the nanoparticle boundary and enter the neighboring materials[3,4] which is found to be an important process useful for a diverse range of applications such as photovoltaics,[5,6] photocatalysis,[3,7,8] nano-scale imaging,[9] and photodetection related applications.[10]

Generation of hot electrons in any nano-scale particle is influenced by the localised surface plasmon induced internal electric field and the quantum mechanical motion of electrons inside the nanoparticle, both of which depend on factors such as the shape, dimensions and composition of the particle in addition to the properties of the surrounding environment and the frequency of the incident radiation.[3,11–16] Therefore precise control of the size and shape of nanoparticles allows us to tailor their hot electron injection behaviour to satisfy the requirements of different applications.

Porous metallic nanomaterials such as nanoshells, nanocages and nanotubes have attracted much attention due to their unique hollow structure and large surface area to volume ratio[17] compared with the solid metal nanostructures. Specifically, nanotubes possess specific optical and geometric properties that are useful for many hot electron based applications.

In solar energy harvesting applications, typically semiconductor materials absorb photons from solar radiation generating electron–hole pairs, causing a current flow in a connected circuit or fuelling the catalytic activity of chemical reactions.[3,7,8] A bottleneck in this process is that the incident photon energy should be higher than the semiconductor bandgap energy for this process to take place, which critically limits its efficiency since the solar spectrum is mostly composed of visible and near-infrared photons having lower energy than typical semiconductor bandgaps. In contrast, hot electrons in plasmonic nanoparticles can be generated and transferred to the conduction band of a semiconductor in contact more easily even for low energy photons than direct electron excitations in the semiconductor.[5,6] Typically for energy harvesting applications nanostructure configurations that absorb energy in the visible and near-infrared region and produce hot electrons are suitable.[18–20] The absorption peaks of nanotubes can be easily tuned to these frequencies using their inner to outer radius ratio, making them suitable for such applications.

Nanotubes show a large surface area to volume ratio compared to solid nanoparticles such as spheres, rods or cubes, making them

[a] *Advanced Computing and Simulation Laboratory (AχL), Department of Electrical and Computer Systems Engineering, Monash University, Clayton, Victoria 3800, Australia. E-mail: chathurangi.kumarasinghe@monash.edu, malin.premaratne@monash.edu*
[b] *Jet Propulsion Laboratory, California Institute of Technology, Pasadena, CA 91109, USA*
[c] *The Institute of Optics, University of Rochester, Rochester, New York 14627, USA*

Published on 09 June 2016. Downloaded by University of Rochester on 07/07/2016 20:32:32.

ideal for applications such as hot electron based sensing and catalytic activities. For sensing applications a high degree of surface contact with the surrounding is desired to sense changes in any environmental parameter. When considering catalytic activities more contact with the reactants can speed up reactions.

Autonomous nanomotors can be driven by recoiling gas bubbles generated by chemical reactions in hollow nanostructures such as nanotubes.[21] For such applications, in addition to the ability to control the rate easily and quickly, directional emitting of outputs from catalytic decomposition of fuels is desired,[21–23] which are properties seen in nanotubes.

Hot electron extraction requires successful charge separation and migration of these carriers to the surface, where they can be extracted for useful work. Theoretical and experimental analysis highlights two main challenges, (1) lack of contact between the electron acceptor, plasmonic nanoparticles, semiconductor and electron donor and (2) ultra-fast energy dissipation of hot electrons before injection into the semiconductor, for efficient charge extraction from plasmonic nanoparticles. Nanotubes have a large contactable surface area. Moreover, the hollow nature of nanotubes allows its inner surface to have contact with the outside media such as electron donor or accepter solutions, giving easier and shorter transfer path for hot electrons radially through the nanoparticle.

In addition to the above-mentioned properties, nanoparticles with cylindrical symmetry show uniform energy absorption for light polarised in any plane perpendicular to its longitudinal axis. Uniform absorption under light polarised in many directions results in stable performance which is important for designing hot electron based nanoelectronic devices such as transistors[24] and current direction switching devices.[25]

In the literature, the hot electron injection behaviour of nanoparticles with shapes such as spheres, cubes[11,26,27] and rods[12] have been analysed in detail. These solid nanostructures have a small surface to volume ratio resulting in reduced contact with the donor–receiver solutions and longer hot electron traversal lengths before extraction, restraining electron transfer at the interface between the nanostructure and the electron donor or receiver. Spherical shells[26] are symmetric and allow easy tuning of the electron injection rate at low frequencies, however they have lower exposed surface area compared to a nanotube because the inner surface is not exposed. Nanopallets[27] have a good surface area to volume ratio, however they fail to perform uniformly at different electric field angles. Therefore nanotubes have a unique combination of properties useful for many hot electron based applications even though they have not been studied so far.

In small nanoparticles, the absorption of radiation is more dominant than scattering leading to higher efficiency of hot electron generation. Furthermore, the injection efficiency is high when the distance the hot electrons have to travel to reach the metal–semiconductor boundary is relatively small so that they have less opportunity to lose energy through different relaxation processes along the migration path. For this reason, smaller nanoparticles can be expected to have higher efficiencies than their larger counterparts when it comes to hot electron injection. It has been shown theoretically for a nanopallet that electron injection efficiencies reduce with increasing pallet width.[27]

Typically, Fowler's theory[28] or an extended version of it[29–31] is used to explain photoemission from a metal to a semiconductor. It assumes an isotropic electron momentum distribution inside the metal. For small nanoparticles with dimensions less than the electron mean free path,[32] this assumption is not suitable, which is the case covered in the analysis presented here. The electron mean free path for silver and gold has reported values of 50 nm and 40 nm, respectively, at energies close to the Fermi energy.[33,34] There are improved versions that add experimentally decided factors into Fowler's theory to get better results.

An alternative is to use an *ab initio* approach based on the density functional theory in which detailed shape and size dependent potential information inside the nanoparticle is taken into account by treating the whole system as a quantum-mechanical many-body problem in order to calculate the rates of hot-electron generation and injection. However, due to its high computationally intensive nature this approach is limited to nanoparticles of size less than 5 nm. Moreover, such a detailed numerical analysis will lead to loss of insight that is very valuable to engineer practical devices and systems. For this reason, we have adopted a much simpler single-electron model, which assumes a non-interacting electron gas confined under a uniform background potential to analyse the hot electron dynamics of nanotubes. This method is suitable for situations where electrons behave as a free-electron gas under a uniform background potential such as in metals. This model has been successfully adopted for other geometries such as nanopallets, nanocubes[11,27] and nanorods,[12] and its results have been successfully matched with detailed density functional theory calculations for nanospheres.[26]

Using a non-interacting, single electron method, we have derived an analytical expression for the size and shape dependent hot electron injection rate for a metallic nanotube with thickness less than electron's mean free path and analysed the hot electron behaviour under varying geometric parameters and frequencies. We have compared our results with the extended Fowler's theory and shown that it fits for nanotubes when the thickness is high.

2 Model

As shown in Fig. 1, we consider a metallic nanotube with outer radius a, inner radius b and length L along the z axis. Its inner boundary is in contact with a thin semiconductor layer creating a potential barrier of $e\phi_B$ between its conduction band and the conduction band of the metal nanotube. This composite nanoparticle is in contact with an electron donor–receptor solution and light of frequency ω is incident on the nanotube with its electric field $\mathbf{E}_0$ oriented perpendicular to the z axis.

The perturbing potential generated by the external illumination is considered as a weak physical disturbance. Therefore the energy levels and eigenstates for an electron in the nanoparticle are not expected to deviate too much from their unperturbed values. By applying perturbation theory to the system, the time-dependent

 This journal is © the Owner Societies 2016

Published on 09 June 2016. Downloaded by University of Rochester on 07/07/2016 20:32:32.

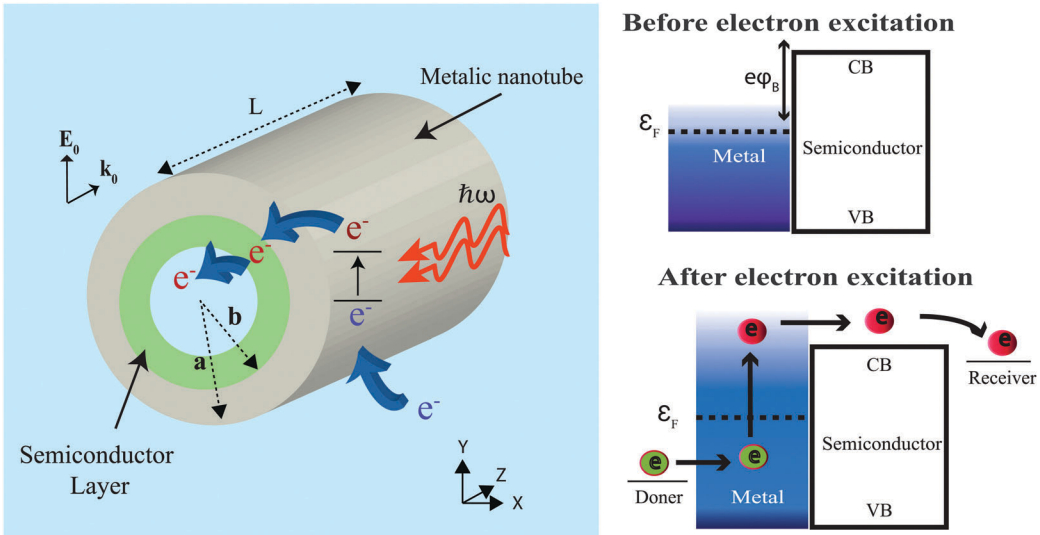

Fig. 1 Schematic showing the generation of hot electrons inside an optically excited metal nanotube (outer radius = a, inner radius = b and length = L) and their injection to the semiconductor in contact over the Schottky barrier formed at the metal–semiconductor interface. The incident light (with photon energy $\hbar\omega$) is propagating in the direction of the wave vector $\mathbf{k}_0$ with its electric field $\mathbf{E}_0$ perpendicular to the longitudinal axis of the nanotube. The energy band diagrams before and after the optical excitation is shown to the right. $e\phi_B$ is the energy difference between the Fermi energy of the metal ($\mathscr{E}_F$) and the conduction band of the semiconductor.

transition probability for an electron in a nanoparticle from an initial state i to a final state f under an external perturbation $V'(\mathbf{r},t)$ can be written as (Fermi's golden rule),[35,36]

$$P_{if}(t) = \left| -\frac{j}{\hbar}\int_0^t \chi_{i,f}\exp(j\omega_{fi}t')\mathrm{d}t' \right|^2, \quad (1)$$

where

$$\chi_{i,f} = \langle \Psi_f(\mathbf{r})|V'(\mathbf{r},t')|\Psi_i(\mathbf{r})\rangle. \quad (2)$$

The variable $\hbar$ is the reduced Planck's constant, j is the unit imaginary number, t is the time measured from the start of the perturbation, $\psi_f(\mathbf{r})$ and $\psi_i(\mathbf{r})$ represent an electron's wave functions in the final and the initial states at position $\mathbf{r}$, respectively, and $\hbar\omega_{fi}$ is the energy difference between these two states. The rate of electron excitation from the state i to f ($\mathbb{R}_{if}(\omega)$) can be obtained by taking the derivative of $P_{if}(t)$ with respect to time. For a sinusoidal perturbation at frequency ω, *i.e.* $V'(\mathbf{r},t) = V'(\mathbf{r})[\exp(j\omega t) + \exp(-j\omega t)]$, this rate is found to be[26,27]

$$\mathbb{R}_{if}(\omega) = \frac{2\pi}{\hbar}\left|\chi_{i,f}\right|^2\delta(\mathscr{E}_f - \mathscr{E}_i - \hbar\omega), \quad (3)$$

where $\mathscr{E}_i$ and $\mathscr{E}_f$ are eigen-energies of the initial and the final states of the transition and $\delta(\mathscr{E}_f - \mathscr{E}_i - \hbar\omega)$ is the Dirac's delta function.

In deriving eqn (3) from eqn (1) we have assumed that the duration of the perturbation t is much greater than the electron thermalisation time Γ associated with electron–electron collisions.[2,36] This allows us to use the approximation

$$\lim_{t\to\infty}\frac{\sin^2((\omega_{fi}-\omega)t/2)}{(\omega_{fi}-\omega)^2t^2/4} = \frac{2\pi\hbar}{t}\delta(\mathscr{E}_f - \mathscr{E}_i - \hbar\omega). \quad (4)$$

By summing $\mathbb{R}_{if}(\omega)$ over all possible initial and final electron states and accounting for the electron availability in the states, the transfer rate of hot electrons from a metallic nanotube to a semiconductor in contact can be obtained as,

$$\mathbb{R}(\omega) = \frac{4}{\Gamma^2}\sum_i\sum_f\left|\chi_{i,f}\right|^2\left[\frac{1}{(\hbar\omega - \mathscr{E}_f + \mathscr{E}_i)^2 + (h/\Gamma)^2} + \frac{1}{(\hbar\omega + \mathscr{E}_f - \mathscr{E}_i)^2 + (h/\Gamma)^2}\right]f_F(\mathscr{E}_i,T)(1 - f_F(\mathscr{E}_f,T)) \quad (5)$$

with $f_F(\mathscr{E}_k,T)$ indicating the Fermi distribution associated with an electron of energy $\mathscr{E}_k$ at temperature T. Variable h is the Planck's constant. The multiplication factors $f_F(\mathscr{E}_i,T)$ and $(1 - f_F(\mathscr{E}_f,T))$ account for the probability of finding an electron in the initial state i and the probability of finding the final state f empty during a transition, respectively. This equation has been multiplied by a factor of 2 to account for electron's spin degeneracy. This is the general formula for calculating the hot electron generation rate in nanoparticles and in the following sections we customise this for a nanotube.

2.1 Perturbing potential inside the nanotube

Let the time-dependent external electric field $\mathbf{E}_0[\exp(j\omega t) + \exp(-j\omega t)]$ be linearly polarised in a plane perpendicular to the longitudinal axis z of the nanotube as shown in Fig. 1. According to Maxwell's equations, the electric field vector inside the particle, $\mathbf{E}(\omega)$, can be related to the potential inside the particle as $\mathbf{E}(\omega) = -\nabla\phi(r,\omega)$.[37] The internal electric field can be written in terms of the externally applied field $\mathbf{E}_0(\omega)$ as $\mathbf{E}(\omega) = \gamma(\omega)\mathbf{E}_0(\omega)$, where $\gamma(\omega)$ is the electric field enhancement factor. For a nanotube with a thin shell ($a - b \ll a$) and a high aspect ratio ($L \gg a$), when the applied electric field is along the

Published on 09 June 2016. Downloaded by University of Rochester on 07/07/2016 20:32:32.

longitudinal axis, the internal electric field enhancement factor $\gamma(\omega)$ can be written as,[38]

$$\gamma(\omega) = \frac{2\varepsilon_0[(\varepsilon_1(\omega)+\varepsilon_2) - 2(\varepsilon_1(\omega)-\varepsilon_2)p]}{2\varepsilon_2(\varepsilon_1(\omega)+\varepsilon_0) + (1-p)(\varepsilon_2-\varepsilon_1(\omega))(\varepsilon_2-\varepsilon_0)}, \quad (6)$$

where ε_0, $\varepsilon_1(\omega)$ and ε_3 are the permittivity of external medium, the metal the nanotube is made of and the semiconductor in contact respectively. The variable p represents the ratio between the inner to outer radius (*i.e.* $p = b/a$). It is clear from this equation that the field inside the nanotube is uniform and parallel to the external field.

2.2 Energy eigenstates of an electron inside a nanotube

In order to calculate the hot electron generation rate $\mathbb{R}(\omega)$, we have to derive expressions for the wave functions and corresponding eigen energies for electrons inside the cylindrical nanotube by solving the Schrödinger equation.[39,40] In nanostructures made of plasmonic metals such as Ag and Au with non-ultra small dimensions, the behaviour of conduction electrons can be closely approximated as a free-electron gas confined within infinite potential barriers at the boundaries of the particle. This allows us to describe the electronic properties of the particle in terms of a single-electron wave function that extends over the entire particle and vanishes at the boundaries. Considering the symmetry of our system, it is convenient to use the cylindrical coordinates (ρ, ϕ, z) with the z axis taken along the length of the nanotube. A Schrödinger equation for a nanotube can be written as,

$$\left(-\frac{\hbar^2}{2\mu}\nabla^2 + V(\rho,\Phi,z)\right)\Psi_k(\rho,\Phi,z) = \mathscr{E}_k\Psi_k(\rho,\Phi,z), \quad (7)$$

with the confining potential $V(\rho, \Phi, z)$ given by

$$V(\rho,\Phi,z) = \begin{cases} 0 & \text{if } a \geq \rho \geq b \text{ and } L \geq z \geq 0 \\ \infty & \text{otherwise} \end{cases}. \quad (8)$$

The variable μ represents the mass of an electron. Owing to the cylindrical symmetry of the nanotube, the wave function $\Psi_k(\mathbf{r})$ can be separated into three functions, $\psi_{n,m}(\rho)$, $\psi_m(\Phi)$ and $\psi_l(z)$ that represent the radial, azimuthal and longitudinal components of the wave function respectively:

$$\Psi_{l,n,m}(\rho, \Phi, z) = \psi_{n,m}(\rho)\psi_m(\Phi)\psi_l(z), \quad (9)$$

The integers n, l and m are quantum numbers representing the quantum state k. The limits of these quantum numbers will be discussed later in this analysis. By solving the eigenvalue problem after substituting eqn (8) and (9) in eqn (7), and considering the orthonormal properties of the wave function we find the components of the wave function needed for further calculations in the form

$$\psi_l(z) = \sqrt{\frac{2}{L}}\sin\left(\frac{l\pi}{L}z\right), \quad (10)$$

$$\psi_m(\phi) = \frac{1}{\sqrt{2\pi}}\exp(jm\phi), \quad (11)$$

$$\psi_{n,m}(\rho) = \sqrt{\frac{2}{(a-b)\rho}}\sin\left(\frac{n\pi}{a-b}(\rho-b)\right), \quad (12)$$

$$\mathscr{E}_k = \frac{\hbar^2}{2\mu}\left[\frac{n^2\pi^2}{(a-b)^2} + \frac{l^2\pi^2}{L^2} + \frac{m^2}{a^2}\right] \quad (13)$$

where n, m and l are integers with the limits $n > 0$ and $l > 0$. In deriving the expression for the radial wave function given by eqn (12), we have made the assumption that the shell of the nanotube is thin compared to its radius ($a - b \ll a$) and taken as $1/\rho \approx 1/a$. Furthermore, the component of energy with momentum in the radial direction ρ for an electron in state k is found to be

$$\mathscr{E}_{k\rho} = \frac{\hbar^2 n^2\pi^2}{2\mu(a-b)^2}. \quad (14)$$

2.3 Rate of hot electron generation and injection

Substituting expressions (10)–(12) in eqn (2) gives,

$$\chi_{i,f} = \frac{\hbar^2 e E_0^2\gamma(\omega)^2}{\mu(\mathscr{E}_f - \mathscr{E}_i)}\left\{\frac{n_f n_i}{a(a-b)}\frac{\left[b - a(-1)^{(n_i-n_f)}\right]}{(n_f^2 - n_i^2)} + \frac{m_i(m_i-m_f)}{2a}\delta_{n_i,n_f}\right\}\delta_{l_i,l_f}\delta_{|m_i-m_f|,1} \quad (15)$$

where the initial state i and the final state f are defined by quantum numbers $\{n_i, m_i, l_i\}$ and $\{n_f, m_f, l_f\}$ respectively. E_0 is the magnitude of the incident electric field. We have used the orthonormal properties of radial and azimuthal wave functions in simplifying the above expression. Because of the presence of the Kronecker delta function δ_{l_i,l_f} in eqn (15) it is clear that the longitudinal quantum numbers of initial and final states have to be equal *i.e.* $l_i = l_f$ for $\chi_{i,f}$ to be non-zero. Physically, this condition is imposed because the incident electric field is perpendicular to the longitudinal axis of the nanotube and the internal electric field is in the same direction as the applied field. By substituting eqn (15) in (5) the hot electron generation rate is found to be,

$$\mathbb{R}(\omega) = \frac{4\hbar^4 e^2 E_0^2\gamma(\omega)^2}{\mu^2\Gamma}\sum_{n_f}\sum_{n_i}\sum_{m_i}\sum_{m_f}\sum_{l_i}\frac{f_F(\mathscr{E}_i,T)(1-f_F(\mathscr{E}_f,T))}{(\hbar\omega-\Delta\mathscr{E})^2 + (\hbar/\Gamma)^2} \times\left(\frac{n_f n_i\left[b - a(-1)^{(n_i-n_f)}\right]}{a(a-b)(n_f^2-n_i^2)} + \frac{m_i(m_i-m_f)}{2a}\delta_{n_i,n_f}\right)^2\frac{\delta_{|m_i-m_f|,1}}{\Delta\mathscr{E}^2} \quad (16)$$

with $\Delta\mathscr{E}$, the energy difference between states f and i derived from eqn (13) to be,

$$\Delta\mathscr{E} \approx \frac{\hbar^2(n_f^2 - n_i^2)\pi^2}{2\mu(a-b)^2}. \quad (17)$$

The duration of electron excitation under the optical field is much greater than the electron relaxation time (Γ) associated with electron–electron collisions. Under such conditions, electrons achieve local equilibrium within the duration of the laser pulse and the nanoparticle thermodynamic state can be described by

 This journal is © the Owner Societies 2016

Published on 09 June 2016. Downloaded by University of Rochester on 07/07/2016 20:32:32.

one temperature. Therefore the hot electron generation rate is independent of time. The limits of summation for quantum numbers m_i, n_i and l_i can be found by noting that the electron will initially occupy a state below the Fermi level and during the transition it will move to an energy state above the Fermi level.

$$\frac{\sqrt{2\mu\mathscr{E}_F}(a-b)}{\pi\hbar} > n_i > 0, \tag{18}$$

$$a\sqrt{\frac{2\mu}{\hbar^2}\mathscr{E}_F - \frac{n_i^2\pi^2}{(a-b)^2}} > |m_i| \geq 0, \tag{19}$$

$$\frac{L}{\pi}\sqrt{\frac{2\mu}{\hbar^2}\mathscr{E}_F - \frac{n_i^2\pi^2}{(a-b)^2} - \frac{m_f^2}{a^2}} > l_i > 0, \tag{20}$$

The term $\delta_{|m_i-m_f|,1}$ decides the limit for m_f as,

$$m_f = m_i \pm 1. \tag{21}$$

Taking the principle of conservation of energy during absorption into consideration *i.e.* $\mathscr{E}_f \leq \mathscr{E}_i + \hbar\omega$, the limits for n_f can be given as

$$\frac{(a-b)}{\pi}\sqrt{\frac{2\mu}{\hbar^2}(\mathscr{E}_F+\hbar\omega) - \frac{m_f^2}{a^2} - \left(\frac{l_i\pi}{L}\right)^2} > n_f > \frac{\sqrt{2\mu\mathscr{E}_F}(a-b)}{\pi\hbar}. \tag{22}$$

We assume a smooth interface between the metal and the semiconductor. This imposes the condition that the component of electron's momentum normal to the interface should be large enough for the electron to cross the Schottky barrier. However, in practice, imperfections and roughness of this interface can change the direction of momentum of incident electrons and relax this assumption, resulting in a higher injection rate. The electron injection rate $\mathbb{R}(\omega)_{inj}$ from the nanotube to the semiconductor in contact with it can be calculated from $\mathbb{R}(\omega)$ by considering only situations where the excited electrons' radial component of the energy ($\mathscr{E}_{f\rho}$) is sufficient to cross the barrier (*i.e.* $\mathscr{E}_{f\rho} > \mathscr{E}_F + e\phi_B$). When an efficient electron donor and an receptor are available effects from charge building up inside the particle can be neglected. Same as before, the electrons are assumed to occupy states below the Fermi level before excitation. After multiplying by 1/2 to allow for the fact that there is an equal probability for an electron to have its momentum towards the metal–semiconductor interface or in the opposite direction, the electron injection rate can be written as

$$\begin{aligned}\mathbb{R}(\omega)_{inj} &= \frac{4\hbar^4 e^2 E_0^2\gamma(\omega)^2}{\mu^2\Gamma} \\ &\times \sum_{n_f}\sum_{n_i}\sum_{m_i}\sum_{m_f}\sum_{l_i}\frac{f_F(\mathscr{E}_i,T)(1-f_F(\mathscr{E}_f,T))}{(\hbar\omega-\Delta\mathscr{E})^2+(2\pi\hbar/\Gamma)^2} \\ &\times \left(\frac{n_f n_i\left[b-a(-1)^{(n_i-n_f)}\right]}{a(a-b)(n_f^2-n_i^2)} + \frac{m_i(m_i-m_f)}{2a}\delta(n_i,n_f)\right)^2 \\ &\times \frac{\delta_{|m_i-m_f|,1}}{\Delta\mathscr{E}^2}\end{aligned} \tag{23}$$

with the limit for the quantum number n_f given by

$$\begin{aligned}&\frac{(a-b)}{\pi}\sqrt{\frac{2\mu}{\hbar^2}(\mathscr{E}_F+\hbar\omega) - \frac{m_f^2}{a^2} - \left(\frac{l_i\pi}{L}\right)^2} \\ &> n_f > \frac{\sqrt{2\mu(\mathscr{E}_F+e\phi_B)}(a-b)}{\pi\hbar}.\end{aligned} \tag{24}$$

The limits for other quantum numbers remain the same as for $\mathbb{R}(\omega)$ and are given by eqn (18)–(21).

When there is an efficient electron donor–receptor mechanism in contact with the nanotube boundaries, we can safely assume the probability of finding an occupied state below the Fermi level and finding an empty state above the energy barrier level is approximately unity. After this simplification, the summation over l_i becomes a degeneracy factor that can be written as

$$\sum_{l_i} 1 = \frac{L}{\pi}\sqrt{\frac{2\mu}{\hbar^2}\mathscr{E}_F - \frac{n_i^2\pi^2}{(a-b)^2} - \frac{m_i^2}{a^2}}. \tag{25}$$

The summation over m_f also can be replaced with multiplication by a factor of 2. Electron thermalisation time Γ in the literature is typically around 350 fs[41–43] for plasmonic metals such as Ag and Au. As a result, when compared to the term $(h/\Gamma)^2$, for small $a-b$ the $\Delta\mathscr{E}$ values and the separation between consecutive $\Delta\mathscr{E}$ are much higher (as seen in eqn (17)). Therefore, it can be seen from eqn (20) that electron transitions for which the energy difference between the initial and the final states is close to the photon energy of the incident radiation contribute significantly to the electron injection rate. Therefore we only consider transitions with $\Delta\mathscr{E} \approx \hbar\omega$ and write n_f as

$$n_f = \frac{(a-b)}{\pi}\sqrt{\frac{n_i^2\pi^2}{(a-b)^2} - \frac{(m_i+m_f)}{a^2} + \frac{2\mu\omega}{\hbar}} \tag{26}$$

By considering only the summation terms where $n_i - n_f$ is odd we simplify eqn (16) to

$$\mathbb{R}(\omega)_{inj} = \frac{2e^2\Gamma E_0^2\gamma(\omega)^2}{\mu^2\omega^2\pi^2}\sum_{n_i}\sum_{m_i}\sum_{l_i}\left[\frac{n_f n_i(a+b)}{a(a-b)(n_f^2-n_i^2)}\right]^2 \tag{27}$$

To simplify this further, we substitute $n_f = n_F$ in eqn (27). This is because if we discard the degeneracy, the rate is maximum when both n_i and n_f are maximum. The degeneracy factor calculated from the summation over n_i, m_i and l_i is replaced by the degeneracy when $n_f = n_F - 1$. After these assumptions, we arrive at,

$$\sum_{m_i}\sum_{l_i} 1 \approx \frac{4\pi aL}{(a-b)^2}[2n_F - 1] \tag{28}$$

$$\begin{aligned}\mathbb{R}(\omega)_{inj} &= \frac{2\sqrt{2}e^2}{\pi^3\hbar^3\mu^{3/2}}\frac{E_0^2\Gamma\mathscr{E}_F(\mathscr{E}_F+\hbar\omega)^{0.5}(\hbar\omega-e\phi_B)}{\omega^4} \\ &\times \frac{\gamma(\omega,a,b)^2(b+a)^2L}{a^2(a-b)^2}\end{aligned} \tag{29}$$

It is apparent from this simplified equation that the hot electron injection rate from a nanotube is quadratically dependent on the magnitude of the applied electric field E_0^2 and the electric

Published on 09 June 2016. Downloaded by University of Rochester on 07/07/2016 20:32:32.

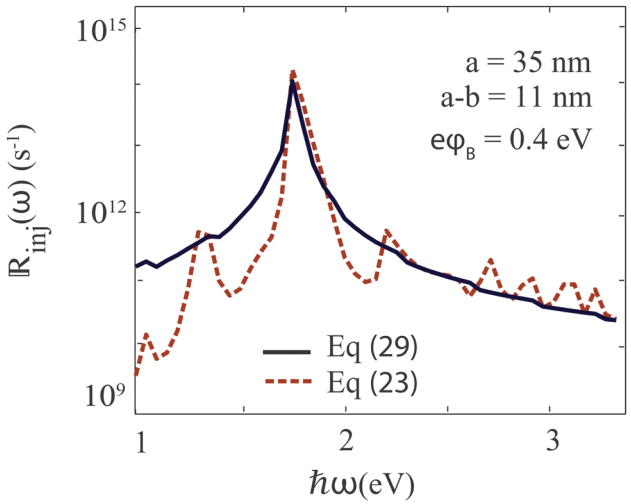

Fig. 2 Electron injection rates calculated from eqn (23) and (29).

field enhancement factor $\gamma(\omega)$. It shows a linear dependency with the electron relaxation time of the metal the nanotube is made of given by Γ and the length of the nanotube L.

In Fig. 2 we have compared the electron injection rates calculated using eqn (23) and (29) for a nanotube. Even though an overestimation of the hot carrier injection rate is visible at low frequencies, eqn (29) describes with sufficient accuracy the hot electron generation rate at high frequencies including its peak value. It should prove useful in practice because of the additional computational effort required for taking the sum over multiple quantum numbers in eqn (23).

3 Results and discussion

In this section we illustrate the energy distribution of generated and injected hot electrons for a nanotube made of Ag consisting of a TiO_2 inner layer and submerged in water. Also we analyse the influence of the geometric properties such as the shell thickness, the ratio between the inner to outer radius and the aspect ratio of the nanotube on the electron injection rate and its internal quantum efficiency using eqn (23) and (29). We have considered the frequency range of 1–3.3 eV in our analysis because the peak values of electron generation and injection for nanotubes are found in this range according to these equations. All of these parameters play an important role in designing a nanotube for hot electron based applications.

TiO_2 is selected as the semiconductor material in contact with the inner boundary of the nanotube as it is a good electron-accepting metal oxide because of a relatively high density of states in its conduction band permitting fast electron injection. Since it has a wide-band-gap of 3.3 eV, it does not absorb radiation below this band-gap value. Therefore, in the frequency range of 1 to 3.3 eV we are investigating, we can neglect any influence from excited electrons in TiO_2 on the electron injection rates.

Silver is selected as the plasmonic metal for the nanotube due to its strong interaction with light. In all calculations we assume the Fermi energy of Ag to be 5.5 eV and the Schottky barrier between Ag and TiO_2 to be 0.4 eV. The complex permittivity of silver is taken from experimental data.[44] To minimize the requirement of external wiring on a nanoscale, typically electron donors and receptors are in the form of a solution in contact with the nanoparticle that causes chemical reactions on the surface. Therefore the surrounding medium is assumed to be water with a relative permittivity of 1.8. Hydrogen ions in water act as the electron receptor resulting in the decomposition of water (H_2O) into oxygen (O_2) and hydrogen gas (H_2) and electrons left behind by this reaction act as electron donors.

The illumination intensity of radiation is taken as 3.6×10^3 W cm^{-2}. For Ag the electron thermalisation time in the literature is typically around 350 fs.[41–43] Due to the availability of an efficient donor–receptor mechanism constantly supplying low energy electrons to the metallic nanotube and fast electron relaxation inside metals, the temperature of electrons T is approximated as the room temperature (300 K).[11]

Fig. 3(a) shows the energy distribution of generated and injected hot electrons calculated from,

$$\mathbb{R}_f(\omega) = \sum_i \mathbb{R}_{if}(\omega) f_F(\mathscr{E}_i, T)(1 - f_F(\mathscr{E}_f), T), \qquad (30)$$

for the specific case of an Ag/TiO_2 nanotube–semiconductor system in water. Photons of 2 eV energy are incident on the silver nanotube such that the electric field is polarized perpendicular to its longitudinal axis. It can be seen that the energy of the generated hot electrons is approximately in the range of $\mathscr{E}_f < \mathscr{E}_F + \hbar\omega$. Most generated hot electrons have energy in the vicinity of the Fermi of the metal ($\mathscr{E}_F$ = 5.5 eV). Only a fraction of them has sufficient energy and correct momentum orientation with respect to the metal–semiconductor interface to cross the Schottky barrier and to enter the semiconductor. A similar behaviour can be observed in other shapes such as nanospheres, nanoshells, nanorods and nanopallets.[12,26,27]

Fig. 3(b) shows the variation of generation and injection rate and the injection efficiency calculated as $\mathbb{R}_{inj}(\omega)/\mathbb{R}(\omega)$, across the spectrum. It is clear that the injection rate can be controlled easily with the frequency of the incident radiation. Also, it can be seen that the injection efficiency varies across the spectrum showing peaks at certain frequencies, which can be considered as an optimum point of operation for this system. The internal quantum efficiency (IQE) of a nanoparticle can be defined as the ratio between the rate of electron injection ($\mathbb{R}(\omega)_{inj}$) and the rate of photon absorption ($\mathbb{R}(\omega)_{ph}$) as

$$\mathbb{R}(\omega)_{ph} = \frac{\mathbb{P}(\omega)_{absorbed}}{\hbar\omega} = \frac{\omega V \Im(\varepsilon_1(\omega))(|\gamma(\omega)|E_0)^2}{2\hbar\omega},$$

where V is the volume of the particle, $\Im(\varepsilon_1(\omega))$ is the imaginary part of the dielectric function of the metal nanotube and $\mathbb{P}(\omega)_{absorbed}$ is the power absorbed.

This quantity is a measure of the energy conversion efficiency of the system and can be used as a figure of merit for comparison among different energy converting systems. In Fig. 4(a) we have plotted the variation of average injection rate per unit volume and average IQE in the range of 1–3.3 eV with varying thickness. It can be seen that both these parameters increase with

 This journal is © the Owner Societies 2016

Published on 09 June 2016. Downloaded by University of Rochester on 07/07/2016 20:32:32.

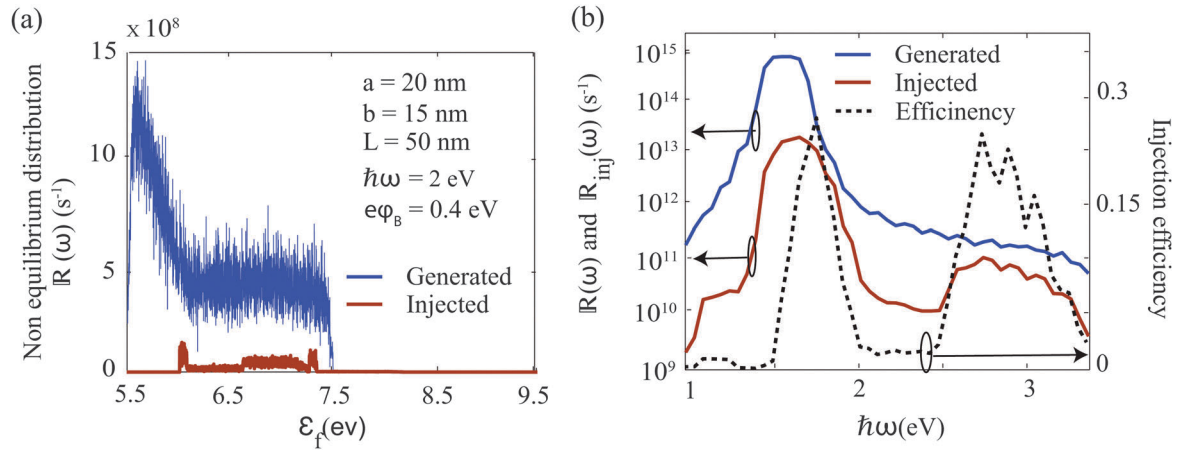

Fig. 3 (a) Energy distribution of generated and injected hot electrons at $\hbar\omega$ = 2 eV for the nanotube shown in Fig. 1. (b) Electron generation and injection rates ($\mathbb{R}(\omega)$ and $\mathbb{R}_{inj}(\omega)$) calculated from eqn (16) and (23) respectively (on a log scale), and injection efficiency ($\mathbb{R}_{inj}(\omega)/\mathbb{R}(\omega)$) as a function of excitation frequency. The incident light is propagating in the direction of the longitudinal axis of the nanotube with its electric field $\mathbf{E}_0$ in a perpendicular plane.

reducing thickness, suggesting thinner nanotubes show better overall performance in this frequency range.

In Fig. 4(b) we have plotted the IQE for nanotubes with two different thicknesses and compared them with the extended Fowler theory predictions given by[28,31,45]

$$\mathrm{IQE} = C\frac{(\hbar\omega - \mathrm{e}\phi_B)^2}{\hbar\omega} \qquad (31)$$

where C is a device specific factor known as the Fowler emission coefficient. It can be seen that our results match well with the Fowler theory predictions particularly for high thickness nanotubes under high excitation frequencies.

Fig. 5 shows the effect of varying the ratio between the inner to outer radius (b/a) while keeping all other factors constant. As seen in Fig. 5(a), this has a significant effect on the injection rate specifically in lower frequencies. In higher frequencies the effect can be considered to be negligible. Moreover, the peaks of electron injection become sharper with increasing b/a. From eqn (6) it can be seen that the electric field enhancement factor ($\gamma(\omega)$) only depends on the ratio $p = b/a$ out of all geometric parameters of the nanotube. Fig. 5(b) shows the variations in γ with the ratio b/a. It can be observed that the position of the peak is blue-shifted with decreasing b/a. It is apparent from Fig. 5(c) that both averaged injection per unit volume and averaged internal quantum efficiency are increasing with increasing b/a.

In practice, nanotubes fabricated can be expected to have irregular, rough surfaces with pits and bumps that can be approximated roughly as an array of small spherical or spheroidal particles, each having its own resonance frequency sitting on a flat surface.[46] If there are only few such irregularities, random peaks can be observed in the field enhancement spectra and the resulting hot electron injection rates. If the surface is highly irregular containing pits and bumps of different

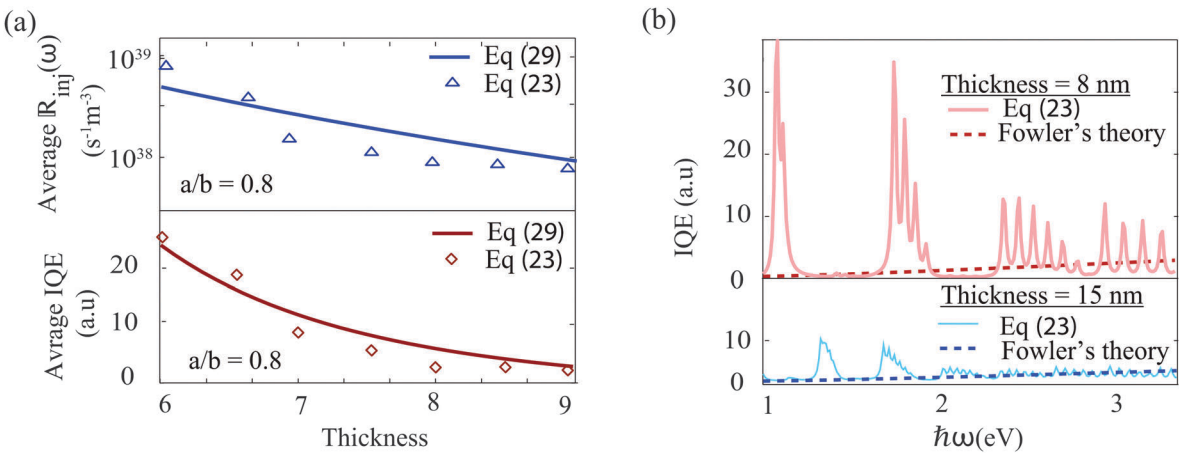

Fig. 4 Effect of varying the thickness of a nanotube while keeping the inner to outer radius ratio and other factors constant. (a) Average hot electron injection rate per unit volume and average quantum efficiency with varying thickness in the frequency range of 1–3.3 eV. (b) Internal quantum efficiency of the hot electron injection from the nanotube calculated from our derivation (solid lines) and from the extended Fowler's theory (dashed lines) given by eqn (31). The length of the nanotube is taken as 100 nm for all calculations and other geometric parameters are indicated in the figure.

Published on 09 June 2016. Downloaded by University of Rochester on 07/07/2016 20:32:32.

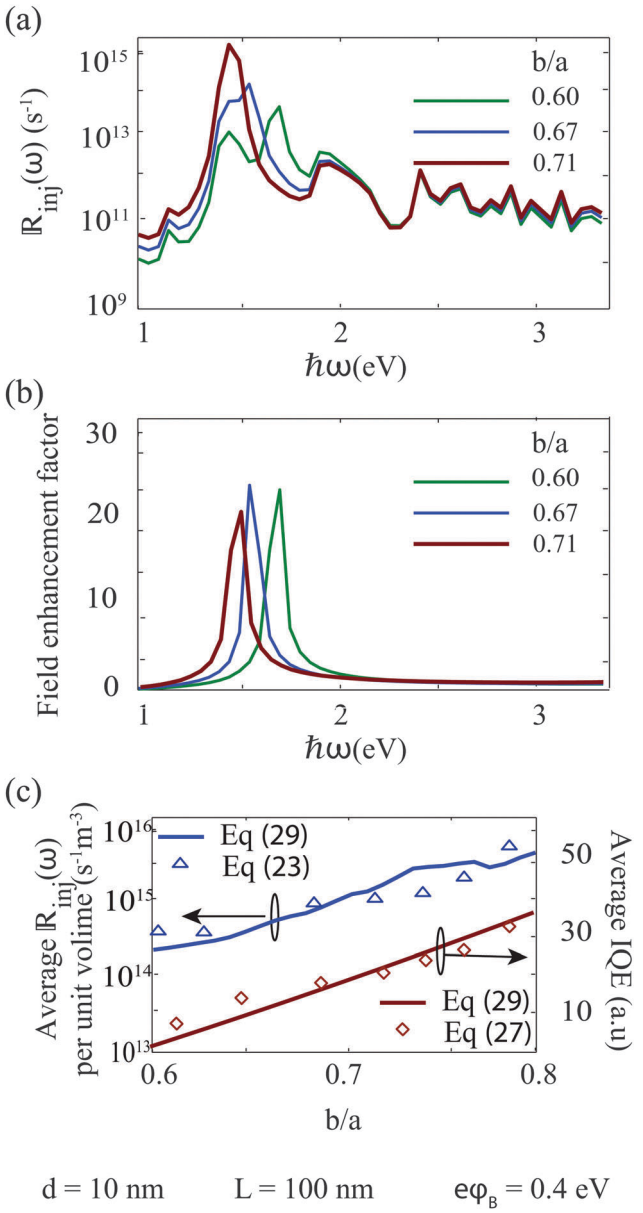

Fig. 5 Effect of varying the inner to outer radius ratio (b/a) of a nanotube while keeping the thickness, length and other factors constant. (a) Electron injection rate *vs.* excitation frequency. (b) Electric field enhancement factor (γ) *vs.* excitation frequency. (c) Averaged electron injection rate and averaged internal quantum efficiency against the b/a ratio in the frequency range of 1–3.3 eV.

sizes and shapes, it can broaden the peaks of the hot electron injection rate.

Fig. 6 summarises the movement of the frequency corresponding to the peak electron injection with the ratio b/a. The peak can be moved between 1–2 eV when b/a is varied from $\sim$0.6–0.95. Since our derivations assume a thin shell restricting the b/a ratio $\sim>0.6$, we have limited our analysis to this range.

Fig. 7 shows the effect of varying the length (L) of the nanotube while keeping all other factors constant. It is apparent that the averaged injection rate is linearly increasing with

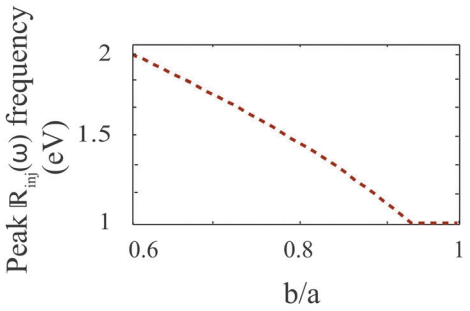

Fig. 6 Effect of varying the inner to outer radius ratio of a nanotube on its peak injection frequency while keeping the thickness and length and other factors constant.

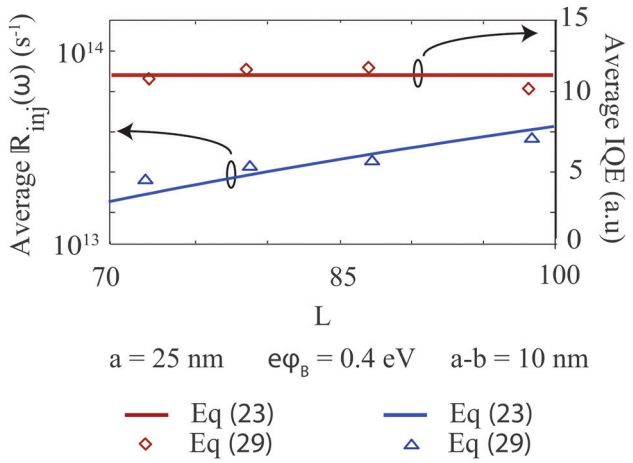

Fig. 7 Effect of varying the length of a nanotube while keeping all other factors constant on averaged electron injection rate and averaged internal quantum efficiency in the frequency range of 1–3.3 eV.

increasing length. However averaged internal quantum efficiency is constant with L.

4 Design guidelines and conclusion

In this article we have derived a simple analytical formula (eqn (29)) for the rate of hot electron injection from a metallic thin shell nanotube to a semiconductor in contact with its inner surface using the single-electron wave function and the corresponding eigen energy states of an electron inside the nanotube. Using this derivation we have analysed how various geometric parameters of a nanotube and the illumination frequency affect the hot electron injection behaviour of a nanotube. Based on the analysis we have identified the following design guidelines.

• Thickness. We have found that reducing the shell thickness of a hollow nanotube can improve the hot electron injection rate and injection efficiency across the spectrum. Also when the shell thickness is reduced, the distance excited electrons have to travel to reach the particle boundary is less, allowing quick transfer of electrons from the donor to the receptor across the shell. This reduces the probability of electrons losing energy

 This journal is © the Owner Societies 2016

Published on 09 June 2016. Downloaded by University of Rochester on 07/07/2016 20:32:32.

before reaching particle boundaries. Therefore thinner nanotubes can be expected to show better performance. However difficulties in fabricating very thin nanotubes and their sustainability against wear and tear have to be considered when deciding a suitable thickness.

• Ratio of the inner to outer radius. We have found that increasing this ratio can increase the hot electron injection rate and its efficiency. Moreover, the frequency corresponding to the peak injection can be tuned in the range 1–2 eV (infra-red and visible regions of the solar spectrum) for nanotubes with thin shells ($b/a < 0.6$) with this ratio. In addition the spectral peaks of injected electrons becomes sharper with increasing b/a. Tunable sharp electron injection peaks are desired for hot electron based sensing applications.

• Length. We have revealed that the average injection rate in the frequency range 1–3.3 eV linearly increases with the length of the nanotube. However, increasing the length beyond an optimum value may have a drawback. Efficient removal of used up electron receptors in contact with the semiconductor attached to the inner surface of the nanotube becomes difficult with increasing length. This is because their circulation through the nanotube from one end to the other takes more time. An efficient electron donor–receptor mechanism is essential to maintain a constant injection rate during the transfer of hot electrons to the semiconductor over sustained periods of time for any hot electron based application. Therefore this may result in a reduction of the overall efficiency, the rate of injection and the stability of the process in practice. The average injection efficiency remains constant with increasing length.

• Frequency of illumination. We have identified that the magnitude of the injection rate of a nanotube can be easily tuned by the frequency of the incident radiation. Therefore, nanotubes are suited for solar energy harvesting applications in the range 1 eV to 3.3 eV where they show highest electric field enhancements and therefore highest injection rates. When considering the spectrum of solar energy reaching Earth's surface, photons in the range of 1.77 eV (700 nm) to 3.10 eV (400 nm) corresponding to the visible region represent 42–43% of the total energy received from the sun.[18–20] Another 50–55% consist of photons in the infra-red region having energies below 1.77 eV (wavelength >700 nm). Only 3–5% have energies in the ultraviolet range with energies above 3.10 eV (wavelength <400 nm). Nanotubes are suited for solar energy harvesting in infra-red and visible regions of the solar spectrum where a large percentage of solar energy is received.

• Semiconductor. It has been experimentally shown that increasing the thickness could drastically reduce the injection rate.[3] This is due to increased resistance the electrons face with increasing thickness while being transferred to the receptor from the metal nanotube resulting in hot electron cooling. However, if the barrier width is too small, tunnelling breakdown can happen,[47] depending on the intensity of the applied electric field, leading to reduced quantum confinement and decreased controllability over the electron flow. Furthermore, difficulties in fabricating very narrow semiconductor layers inside a nanotube must also be considered.

Materials that support high local electric field enhancements in the visible and near infra-red regions (such as Ag, Au and Cu) are suitable for constructing the nanotube.

For different hot electron based applications different hot electron injection behaviour is considered optimum. Our analysis and results provide the much needed theoretical background for development and optimization of nanotubes for various hot-electron based applications. The hollow nature of nanotubes offer an additional source of tunability over non-hollow counterparts since the photon absorption peak can be controlled by varying the inner to outer radius ratio which may prove important for the sensing and design of hot electron based electronic devices. In addition to this nanotubes provide a larger contact area and controlled output direction important for hot electron based catalysis and sensing applications. Also the thin shell of nanotubes allows quick transfer of electrons from the donor to the acceptor through the nanostructure, reducing the probability of electrons losing energy before reaching particle boundaries. Along with these properties, the ability to generate hot electrons with almost constant efficiency over a wide range of incident electric field angles makes nanotubes unique among other symmetrical and non-symmetrical nanoparticle shapes.

Acknowledgements

The work of C. S. K. is supported by the Monash University Institute of Graduate Research. The work of M. P., S. D. G. and G. P. A. is supported by the Australian Research Council, through its Discovery Grant DP140100883.

References

1 G. Schmid, *Nanoparticles: from theory to application*, John Wiley & Sons, 2011.
2 M. Kaviany, *Heat transfer physics*, Cambridge University Press, 2014.
3 S. Mubeen, J. Lee, N. Singh, S. Krämer, G. D. Stucky and M. Moskovits, *Nat. Nanotechnol.*, 2013, **8**, 247–251.
4 N. Zhang, S. Liu, X. Fu and Y.-J. Xu, *J. Phys. Chem. C*, 2011, **115**, 9136–9145.
5 Y. K. Lee, C. H. Jung, J. Park, H. Seo, G. A. Somorjai and J. Y. Park, *Nano Lett.*, 2011, **11**, 4251–4255.
6 D. Conklin, S. Nanayakkara, T.-H. Park, M. F. Lagadec, J. T. Stecher, X. Chen, M. J. Therien and D. A. Bonnell, *ACS Nano*, 2013, **7**, 4479–4486.
7 J. Lee, S. Mubeen, X. Ji, G. D. Stucky and M. Moskovits, *Nano Lett.*, 2012, **12**, 5014–5019.
8 C. Gomes Silva, R. Juárez, T. Marino, R. Molinari and H. Garcia, *J. Am. Chem. Soc.*, 2010, **133**, 595–602.
9 A. Giugni, B. Torre, A. Toma, M. Francardi, M. Malerba, A. Alabastri, R. P. Zaccaria, M. Stockman and E. Di Fabrizio, *Nat. Nanotechnol.*, 2013, **8**, 845–852.
10 N. Landy, S. Sajuyigbe, J. Mock, D. Smith and W. Padilla, *Phys. Rev. Lett.*, 2008, **100**, 207402.

Published on 09 June 2016. Downloaded by University of Rochester on 07/07/2016 20:32:32.

11 A. O. Govorov, H. Zhang, H. V. Demir and Y. K. Gunko, *Nano Today*, 2014, **9**, 85–101.
12 C. S. Kumarasinghe, M. Premaratne, Q. Bao and G. P. Agrawal, *Sci. Rep.*, 2015, **5**, 12140.
13 N. Das, F. F. Masouleh and H. R. Mashayekhi, *IEEE Trans. Nanotechnol.*, 2014, **13**, 982–989.
14 F. F. Masouleh, N. Das and S. M. Rozati, *Opt. Quantum Electron.*, 2015, **47**, 1477–1485.
15 W. Zhu, I. D. Rukhlenko and M. Premaratne, *Appl. Phys. Lett.*, 2012, **101**, 031907.
16 I. D. Rukhlenko, A. Pannipitiya and M. Premaratne, *Opt. Lett.*, 2011, **36**, 3374–3376.
17 X. Guo, W. Ye, H. Sun, Q. Zhang and J. Yang, *Nanoscale*, 2013, **5**, 12582–12588.
18 C. Gueymard, D. Myers and K. Emery, *Sol. Energy*, 2002, **73**, 443–467.
19 J. Tabak, *Solar and geothermal energy*, Infobase Publishing, 2009.
20 A. E. Dixon and J. D. Leslie, *Solar Energy Conversion: An Introductory Course*, Elsevier, 2013.
21 Y. Mei, A. A. Solovev, S. Sanchez and O. G. Schmidt, *Chem. Soc. Rev.*, 2011, **40**, 2109–2119.
22 L. F. Valadares, Y.-G. Tao, N. S. Zacharia, V. Kitaev, F. Galembeck, R. Kapral and G. A. Ozin, *Small*, 2010, **6**, 565–572.
23 S. Sanchez, A. A. Solovev, S. Schulze and O. G. Schmidt, *Chem. Commun.*, 2011, **47**, 698–700.
24 Z. Fang, Y. Wang, Z. Liu, A. Schlather, P. M. Ajayan, F. H. Koppens, P. Nordlander and N. J. Halas, *ACS Nano*, 2012, **6**, 10222–10228.
25 C. S. Kumarasinghe, M. Premaratne, S. D. Gunapala and G. P. Agrawal, *Sci. Rep.*, 2016, **6**, 21470.
26 A. Manjavacas, J. G. Liu, V. Kulkarni and P. Nordlander, *ACS Nano*, 2014, **8**, 7630–7638.
27 A. O. Govorov, H. Zhang and Y. K. Gunko, *J. Phys. Chem. C*, 2013, **117**, 16616–16631.
28 R. H. Fowler, *Phys. Rev.*, 1931, **38**, 45.
29 J. Cohen, J. Vilms and R. J. Archer, *Investigation of semiconductor Schottky barriers for optical detection and cathodic emission*, Dtic document technical report, 1968.
30 V. L. Dalal, *J. Appl. Phys.*, 1971, **42**, 2274–2279.
31 J. M. Mooney and J. Silverman, *IEEE Trans. Electron Devices*, 1985, **32**, 33–39.
32 M. W. Knight, Y. Wang, A. S. Urban, A. Sobhani, B. Y. Zheng, P. Nordlander and N. J. Halas, *Nano Lett.*, 2013, **13**, 1687–1692.
33 K. W. Frese and C. Chen, *J. Electrochem. Soc.*, 1992, **139**, 3234–3243.
34 A.-M. Dowgiallo, A. M. Schwartzberg and K. L. Knappenberger Jr, *Nano Lett.*, 2011, **11**, 3258–3262.
35 D. Griffiths, *Introduction to Quantum Mechanics*, Pearson Prentice Hall, 2005.
36 N. Zettili, *Quantum mechanics: concepts and applications*, John Wiley & Sons, 2009.
37 M. Premaratne and G. Agrawal, *Light Propagation in Gain Media: Optical Amplifiers*, Cambridge University, 2011.
38 A. E. DePrince and R. J. Hinde, *Nanoscale Res. Lett.*, 2010, **5**, 592–596.
39 G. Grynberg, A. Aspect and C. Fabre, *Introduction to quantum optics: from the semi-classical approach to quantized light*, Cambridge university press, 2010.
40 D. Weeraddana, M. Premaratne and D. L. Andrews, *Phys. Rev. B: Condens. Matter Mater. Phys.*, 2015, **92**, 035128.
41 R. H. Groeneveld, R. Sprik and A. Lagendijk, *Phys. Rev. B: Condens. Matter Mater. Phys.*, 1995, **51**, 11433.
42 C. Voisin, N. Del Fatti, D. Christofilos and F. Vallee, *J. Phys. Chem. B*, 2001, **105**, 2264–2280.
43 C. Voisin, D. Christofilos, N. Del Fatti, F. Vallée, B. Prével, E. Cottancin, J. Lermé, M. Pellarin and M. Broyer, *Phys. Rev. Lett.*, 2000, **85**, 2200.
44 P. B. Johnson and R.-W. Christy, *Phys. Rev. B: Condens. Matter Mater. Phys.*, 1972, **6**, 4370.
45 A. Rogalski, Infrared photon detectors/Antoni Rogalski; with contributions by Masafumi Kinata...[*et al.*], Bellingham, WA: SPIE Optical Engineering Press, c1995., 1995.
46 F. Lee, K. Lee, S. Lai, Y. Cheng and T. Hsu, *Solid State Commun.*, 1987, **63**, 299–302.
47 K. Wu, W. E. Rodríguez-Córdoba, Y. Yang and T. Lian, *Nano Lett.*, 2013, **13**, 5255–5263.

 This journal is © the Owner Societies 2016